·论著·

比较氢质子磁共振波谱和正反相位 MRI 成像在骨髓脂肪沉积中的价值

张灵艳 李绍林* 郝帅
南方医科大学第三附属医院广东省骨科研究院影像科,广东 广州 510630

中图分类号:R445 **文献标识码**:A **文章编号**:1006-7108(2015)06-0691-06

摘要:**目的** 探讨氢质子磁共振波谱(^{1}H-MRS)和双回波正反相位(in-phase and out-phase)MRI 成像技术在骨髓脂肪沉积中的价值,并比较两种方法一致性。**方法** 前瞻性选择经我院双能 X 线骨密度测量仪(DXA)确诊的 38 例骨质疏松者及 30 例骨量正常者分别行 MRI 常规检查、^{1}H-MRS 及双回波正反相位成像,并收集资料,分别测量 L2 椎体的反相位和正相位信号比值(SIR)、水脂比(LRW)和脂肪分数(FF)。采用 t 检验比较两组的 SIR、LRW 及 FF 差异;采用 ROC 曲线分析 SIR 值、LRW 及 FF 对骨质疏松诊断效能,并初步确定骨质疏松各指标诊断阈值;Kolmogorov-Snimov 法进行正态性检验,资料符合正态分布,选择 pearson 相关分析分别检验 SIR 与 LRW 和 FF 的相关性。**结果** 得到横轴位和矢状位各 68 幅 MRI 腰椎正反相位图,得到 68 幅单体素 MRS 波谱图,骨质疏松组 SIR 值、LWR 及 FF 分别为 0.498±0.160、3.677±3.093、0.732±0.176,骨量正常组 SIR 值、LWR 及 FF 分别为 0.350±0.971、2.094±1.892、0.573±0.211,两组间 SIR、LWR FF 差异均有统计学意义(t 值分别为 6.404、2.035、2.738,*P* 值均 <0.05);正反相位所测 SIR 区分骨质疏松的 ROC 曲线下面积为 0.784,SIR 阈值为 0.3850,灵敏度 78.9%,特异度为 66.7%。MRS 中 LWR、FF 区分骨质疏松的 ROC 曲线下面积分别为 0.706、0.740,阈值分别为 2.063、0.674,灵敏度分别为 75.0%,79.2%,特异度分别为 71.4%、72.4%。*Pearson* 相关分析 SIR 与 LRW 和 FF 的 r 值和 *P* 值,结果 *P* 值均 <0.05。**结论** ^{1}H-MRS 和正反相位 MRI 两种方法均能提供腰椎骨髓脂肪沉积定量信息,可以无创、快速协助诊断骨质疏松,二者指标间有相关性。

关键词:磁共振波谱;正反相位;骨质疏松;骨髓脂肪;信号

Comparison of 1H-MRS imaging and in-phase and out-phase MR imaging in the detection of bone marrow fat deposition

ZHANG Lingyan, LI Shaolin, HAO Shuai
Department of Medical Imaging, the 3rd Affiliated Hospital of Southern Medical University, Guangzhou 510630, China
Corresponding author: LI Shaolin, Email: 18926191928@189.cn

Abstract: **Objective** To explore the diagnostic value of 1H proton MRS and in-phase and out-phase MRI for bone marrow fat deposition (BMFD), and to compare the consistency of two methods. **Methods** Thirsty-eight patients who were diagnosed with osteoporosis using DXA and 30 people with normal bone mass were enrolled in this study. All the 68 subjects underwent MRI regular examination, MRS, and in-phase and out-phase MRI. SIR, LRW, and FF of L2 vertebra were measured. SIR, LRW, and FF between the two groups were compared using Student t test. Diagnostic accuracy of SIR, LRW, and FF for osteoporosis were analyzed using ROC curve, and the diagnostic threshold of these indicators for osteoporosis was determined. By the use of Kolmogorov-Snimov normality test, the data were proved to be normally distributed. The correlations among SIR, LRW, and FF were assessed with Pearson analysis. **Results** Sixty-eight axial and sagittal MRI in-phase and out-phase MR images of the lumbar spine and 68 single voxel MRS images were obtained. SIR, LWR, and FF in osteoporosis group were 0.498±0.160, 3.677±3.093, and 0.732±0.176, respectively. SIR, LWR, and FF in normal bone mass group were 0.350±0.971, 2.094±1.892, and 0.573±0.211, respectively. There were statistically significant differences in SIR, LWR, and FF between the two groups (t values were 6.404, 2.035, and 2.738 respectively, *P* <0.05). The area (measured with the SIR deferential point) under ROC curve was

基金项目:南方医科大学第三附属医院广东省骨科研究院科技项目院长基金(B201012)
* 通讯作者:李绍林,Email:18926191928@189.cn

0.784. Using the SIR value of 0.3850 as the ROC cut off point, the diagnostic sensitivity and specificity were 78.9% and 66.7%, respectively. In MRS, using the value 2.063 of LWR and 0.674 of FF as the cutting off points, the area under ROC curve was 0.706 and 0.740, the diagnostic sensitivity was 75.0% and 79.2%, and the diagnostic specificity was 71.4% and 72.4%, respectively. The result of correlation analysis between SIR, LRW, and FF using Pearson correlation showed $P < 0.05$. **Conclusion** Both 1H-MRS and in-phase and out-phase MRI can provide information of bone marrow fat deposition in the lumbar spine and help to achieve quick and non-invasive osteoporosis diagnosis. There is correlation between the indicators of the two methods.

Key words: Magnetic resonance spectroscopy; In-phase and out-phase; Osteoporosis; Bone marrow fat; Signal

骨质疏松症正在成为全球性威胁人体健康疾病,研究认为腰椎椎体最能体现全身骨质状态,而椎体内脂肪沉积同骨质疏松关系密切,随着 MRI 成像技术的进步,目前已开展 MRI 方法检测骨质疏松患者椎体骨髓脂肪含量,本研究主要比较^{1}H-MRS 和水脂分离的正反相位 MRI 两种方法在骨髓脂肪沉积方面的作用,为临床无创快速诊断骨质疏松提供新的思路。

1 材料和方法

1.1 临床资料

前瞻性分析 2013 年 5 月至 2013 年 9 月期间,于我院脊柱骨科和体检中心就诊和体检人群 300 例中随机选择 68 例,根据在我院行腰椎 DXA 检查结果,即根据 T 值 > −1 和 T < 值 −2.5 分为骨量正常和骨质疏松组,其中,经 DXA 测量腰椎确认为骨质疏松 38 例,骨量正常 30 例,排除肿瘤、新鲜骨折、感染及其他代谢性疾病患者。骨量正常组年龄 20 ~ 52 岁,平均 34.3 岁,包括男 16 例,女 14 例。骨质疏松组年龄 42 ~ 73 岁,平均 63.2 岁,包括男 16 例,女 22 例; DXA、^{1}H-MRS、正反相位成像三种检查尽量于同一天最迟未超过 5 天间隔,本研究所有参与研究者检查前都签署了知情同意书。

1.2 常规 MRI 检查

采用 Philips Achieva 1.5TMR 成像仪,15 通道脊柱相控阵线圈,分别行矢状位和横轴位 T2WI 及矢状位 T1WI 成像,病人体位采取仰卧位,平静呼吸。扫描参数: 矢状位 T2WI: TR2740ms, TE 100ms, FOV 160 mm × 302 mm, 矩阵 176 × 238, 层间距 0 mm, 层厚 4 mm, 采集次数 2。横轴位 T2WI: TR2308 ms, TE 120 ms, FOV 160 mm × 302 mm, 矩阵 280 × 210, 层间距 0 mm, 层厚 4 mm, 采集次数 2。矢状位 T1WI: TR400ms, TE 8.0 ms, FOV 160 mm × 302 mm, 矩阵 160 × 210, 层间距 0 mm, 层厚 4 mm, 反转角 90°, 采集次数 1。

1.3 双回波正反相位成像

采用 Philips Achieva 1.5TMR 成像仪,行 Dual-FFE 加脂肪抑制扫描,扫描中心位置与轴位 T1WI 脂肪抑制序列一致。扫描参数: T1WI 矢状位双回波成像 TR 150 ms, TE 正相位 4.61 ms; TE 反相位 2.3 ms, FOV 48 cm × 44 cm, 翻转角 90°, 矩阵 256 × 257, 层厚 3.2 mm, 层间距 0 mm, 扫描层数 15; 扫描时间 39.1 s。T1WI 横轴位双回波成像 TR 110 ms, TE 2.5 ms, FOV 480 mm × 440 mm, 翻转角 80°, 矩阵 256 × 217, 层厚 10 mm, 层间距 2 mm, 扫描层数 12; 扫描时间 20.2 s。

1.4 ^{1}H-MRS 检查

采用 Philips Achieva 1.5TMR 成像仪,根据 T2WI 腰椎矢状位成像定位,先进行匀场,不抑水,采用单体素点解析波谱(PRESS)序列, TR2000, TE38, 体素大小: 15cm × 15 cm × 15cm, 翻转角 90°, 采集次数 8, 扫描时间 20 s。激励次数 2。

1.5 图像分析和数据处理

将原始数据传至 Extended MR 后处理工作站,将轴位 T1WI 脂肪抑制图作为解剖定位图,获得正、反回波图像椎体信号强度,图像由 2 名脊椎疾病诊断经验丰富的放射科医师共同评估,根据文献[1],选择正中矢状位 L_2 椎体中心圆形感兴趣区(regions of interesting, ROI),面积为 100 ~ 105 mm^2,尽量避开椎体皮质及血管区,选择计算信号强度比(signal intensity ratio, SIR): SIR = 反回波信号强度/正回波信号强度。MRS 先对波谱进行校正,分别测量位移于 4.65 ppm 的水峰值及位移于 1.3 ppm 处水峰值高度,自动获得脂水比: (LWR = L/W, 脂肪峰高度值/水峰高度值)和脂肪信号分数(FF): FF = LWR/1 + LWR, 以上测量均分别测量 3 次,最后取其平均值。(见图 1)。

1.6 统计学处理

采用统计学软件 SPSS17.0 统计学软件进行统计学处理,分别测量骨质疏松组及骨量正常组的 SIR、LWR 及 FF, 比较采用 t 检验,并分析两组间年龄、性别(性别采用秩和检验)有无差异,采用 ROC

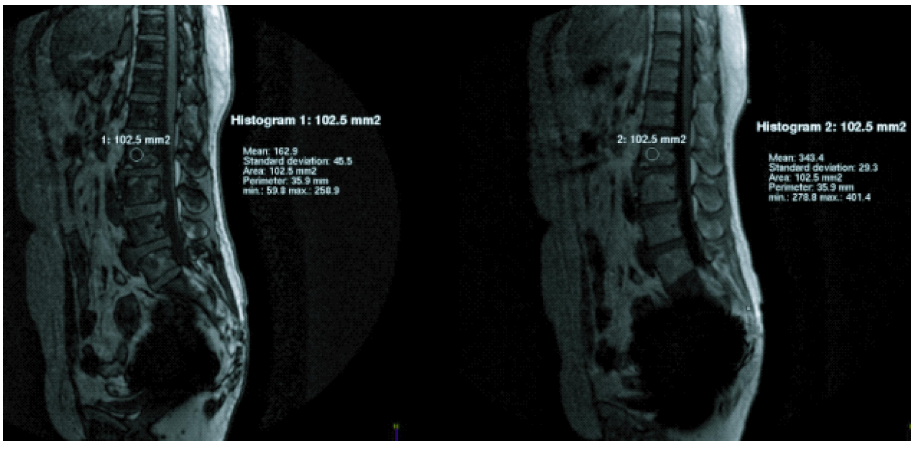

图 1 矢状位反相位(out-of-fase)正相位(infase)图像及测量方法

Fig. 1 The images of out-phase and in-phase MRI and the measuring method.

曲线分析 SIR、FF 及 LWR 诊断骨质疏松的效能,分别计算曲线下面积、测定各自阈值、灵敏度和特异度。Kolmogorov-Snimov 法进行正态性检验,资料符合正态分布,选择 pearson 相关分析采用 person 相关分析检验 SIR 分别与 LRW 和 FF% 的相关性。$P < 0.05$ 为差异有统计学意义。

2 结果

2.1 正反相位 MRI 成像结果

骨质疏松和骨量正常两组 SIR 差异有统计学意义(见表 1)。

表 1 骨质疏松和骨量正常两组 SIR 结果比较($\bar{x} \pm s$)

Table 1 Comparison of the SIR value between osteoporosis group and normal group.

组别	例数(例)	年龄(岁)	SIR
osteoporosis group	38	63.210 ± 8.052	0.498 ± 0.160
normal group	30	38.110 ± 9.373	0.350 ± 0.097
t 值		7.314	2.531
P 值		< 0.01	< 0.01

两组性别之间采用秩和检验两组间 $P > 0.05$,差异无统计学意义。两组年龄差异有统计学意义。

ROC 曲线上,SIR 曲线下面积为 0.784,95 % 可信区间为 0.609 ~ 0.959,SIR 阈值为 0.3850,灵敏度 78.9%,特异度为 66.7%。(图 2)

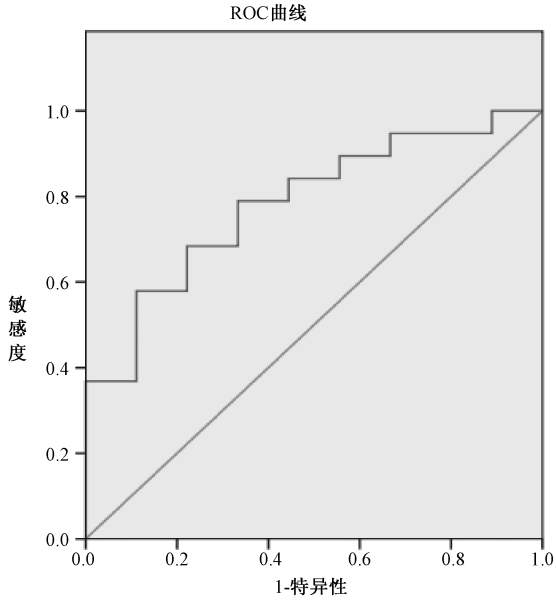

图 2 双回波正反相位 SIR 诊断骨质疏松的 ROC 曲线分析

Fig. 2 ROC curve analysis of SIR value in the diagnosis of osteoporosis.

2.2 MRS 结果

骨质疏松组与骨量正常组之间 FF、LWR 差异有统计学意义(见表 2)。

骨质疏松组与骨量正常两组年龄之间 $P < 0.05$,差异有统计学意义。

ROC 曲线上,FF 曲线下面积为 0.740,95 % 可信区间为 0.591 ~ 0.889,FF% 阈值为 0.674,灵敏度 79.2%,特异度为 72.4%;LWR 曲线下面积为 0.706,95 % 可信区间为 0.550 ~ 0.863,LWR 阈值为 2.063,灵敏度 75.0%,特异度为 71.4%(图 4)

表 2 骨质疏松和骨量正常两组 FF% 、LWR 结果比较($\bar{x} \pm s$)

Table 2 Comparison of FF% and LWR between osteoporosis group and normal group

组别	例数(例)	FF	LWR
osteoporosis group	38	0.732 ± 0.176	3.677 ± 3.093
normal group	30	0.573 ± 0.211	2.094 ± 1.892
t 值		2.738	2.035
P 值		< 0.01	< 0.05

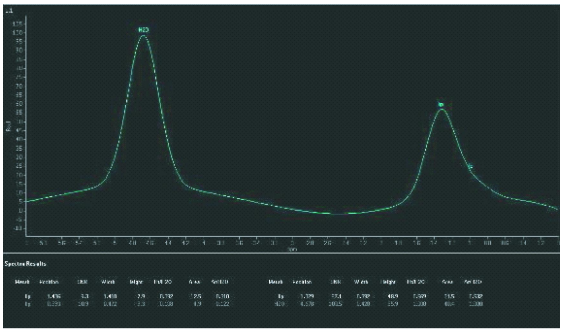

骨量正常者：本例男性，17岁，相应正反相位上SIR0.293
Normal case：Male，17 year old，SIR value 0.293

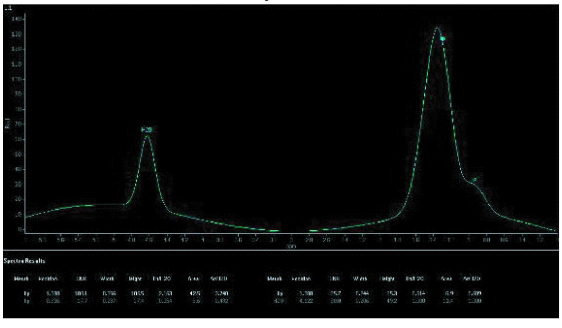

骨质疏松病例：本例男性，53岁，相应正反相位上SIR0.520
Osteoporosis case：Male，53 year old，SIR value 0.520

图 3 波谱图

Fig. 3 Image, X axis, frequency; Y axis, signal intensity

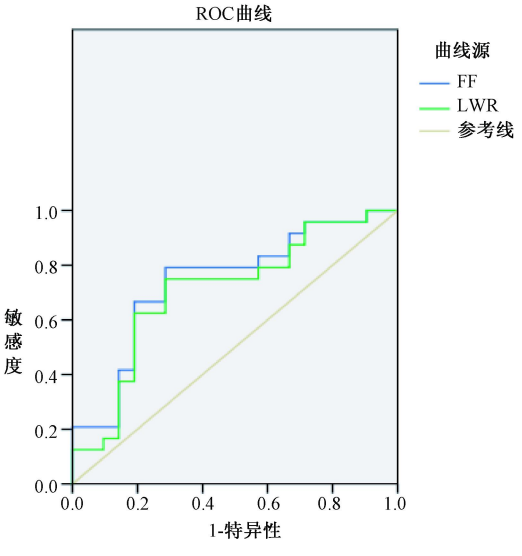

图 4 FF 和 LWR 诊断骨质疏松的 ROC 曲线分析

Fig. 4 ROC curve analysis of FF and LWR in the diagnosis of osteoporosis.

3 讨论

3.1 正反相位 MR 成像、^{1}H-MRS 在骨髓脂肪检测中的应用

双回波成像又叫正反相位成像、脂肪分数成像，是基于水脂分离技术的 Dixon 方法[1,2] 中的一种。其原理利用生物组织内水质子和脂肪质子拉莫尔频率差，通过调节回波时间 TE 做两次采集，第一次采集使得这两种成份横向磁化强度矢量同相位（in-phase），得到的图像信号强度为水与脂肪信号强度之和；第二次采集使得它们的相位相反（out-of-phase），得到的图像信号强度为两者之差的绝对值。水脂分离的正反相位由于具有分离脂肪组织迅速，兼容性较广，信噪比较高和可以定量检测脂肪组织等优点[3]，已经被较广泛应用于腹部脏器尤其肾上腺病变、脂肪肝[4] 等含有水脂成分的病变检测，近年来开始应用到骨髓脂肪组织。^{1}H-MRS 是通过化学位移原理，选择单体素 PRESS 序列，检测脂肪分子和水分子，得到脂肪峰和水峰，脂肪的波峰较复杂，主峰位于 1.3 ppm 处。水峰位于 4.6～4.7（约 4.65 ppm）ppm，高度约为其他波峰的 10 倍，不同年龄阶段，骨髓内脂肪、水分、蛋白质、矿物质等成分含量不断变化，随着年龄增长，椎体内含脂肪的黄骨髓成分逐渐增加，含水分较多的红骨髓相应减少。以往研究表明骨髓的脂肪含量与矿物质密度呈负相关[5,6]。由于 MRS 技术可以精确测量脂肪含量及脂肪与水的比例，从而从细胞层面揭示骨髓脂肪含量在骨质疏松发病机制发挥重要作用[8]。

3.2 本研究结果分析

本研究中骨量正常组年龄偏轻，FF 平均值 0.573，骨质疏松组平均年龄 63 岁，FF 值平均 0.732，本研究结果数值均高于文献中[7] 对不同年龄健康志愿者 L_3 椎体进行脂肪含量测定结果：FF 值从年轻组 0.307 逐渐增高到 60 岁以上年龄组的 0.517。本研究中利用^{1}H-MRS 对骨量正常组 L_2 椎体的骨髓脂肪含量，平均脂肪分数为 0.35，同国外对健康志愿者的 $L_{3,4,5}$ 椎体测量结果 FF 为 0.37（标准误 0.08）研究结果相近[8]，同时研究发现基于水脂分离的 Dixon 技术用于脊椎骨髓脂肪测量重复性较好。有学者[10] 利用 MRI 技术评估腰椎骨髓正常及浸润性疾病表现。以往有关于 MRS 定量研究内脏器官胰腺等器官脂肪含量的报道[11]，但同样的方法不能应用于脊椎部位，因为脊椎骨髓内脂肪分布相对皮下、肌肉及内脏器官更加不均匀，且脂肪含量较少。以往研究脂肪与骨密度关系较多[12-14]，二者显示呈负相关[15]。本研究中 MRS 所测 LWR、FF 与 BMD 间为负相关，同文献报道一致。SIR 同 BMD 之间亦为负相关，可能由于因为随着骨密度减低，伴有骨髓脂肪变性的黄骨髓含量增加，而原来的骨髓

内带有水分子的其他组织如红骨髓因为缺血坏死而减少,因而 SIR 较高[16]。但国外学者[17]通过对 55-60 岁骨质疏松组和骨量正常组的 L_3 椎体分别进行化学位移 MRI 成像(CS-MRI),发现二者统计学差异并不明显,结果表明 CS-MRI 测得的椎体骨髓脂肪信号并不是预测骨质疏松敏感指标。最近国外学者[18]对腰痛病人三维双梯度回波和多梯度回波 MRI 中得出的腰部肌肉脂肪信号分数和从单体素 MR 波谱中得出的分数进行比较研究,得出双回波和多回波 MRI 和波谱的脂肪信号分数一致性较好结论。最近[19]通过对家庭成员包括父亲母亲和女儿的 MRS 和正反相位上检测腰椎骨髓脂肪含量,也得出两种方法具有很强的一致性和相关性结论。

本研究选择腰椎椎体作为 MRS 和正反相位 MRI 两个方法测量目标部位,原因是骨髓脂肪含量主要与骨质疏松有密切关系,而腰椎是用来诊断骨质疏松的常用检查部位,可以反映全身骨矿物质密度。本研究中 MRS 和正反相位 MRI 两个方法通过测量 L_2 骨髓脂肪含量,区分骨质疏松和骨量正常的效能均较高,说明两个方法均有望作为辅助诊断骨质疏松的新方法,为进一步探索骨质疏松的细胞分子水平机制奠定基础。本研究中两个方法所测结果有出现矛盾的时候,分析可能的原因:一椎体内骨髓脂肪分布本身是不均匀的;其二,正反相位 MR 成像会受到部分容积效应的影响和技术本身有约 45% 脂肪含量误差。

3.3 本研究不足与展望

本研究的不足之处在于:1)本研究仅仅测量了一个椎体 L_2 的 SIR,其他腰椎椎体未一一测量,其代表性有待考证。2)样本量较小,尤其骨量正常者年龄均偏小,未包含各年龄段人群。3)本研究所用双回波 MRI 成像方法是 Dixon 方法中之一,目前有两点、三点 Dixon 技术出现,解决了水脂易错换和测量不准确等问题,可以更准确量化脂肪含量,需在本研究基础上进一步深入研究。

【参考文献】

[1] Dixon WT. Simple proton spectroscopic imaging. Radiology, 1984; 153:189-194.

[2] Reeder SB, Wen Z, Yu H, et al. Multicoil Dixon chemical species separation with an iterative least-squares estimation method. Magn Reson Med 2004;51:35-45.

[3] Bley TA, Wieben O, Francois CJ et al. Fat and Water Magnetic Resonance Imaging. J Magn Reson Imaging. 2010,31(1):4-18.

[4] Borra RJ, Salo S, Dean K, et al. Nonalcoholic fatty liver disease: rapid evaluation of liver fat content with in-phase and out-of-phase MR imaging. Radiology 2009,250:130-136.

[5] N. Di Iorgi, M. Rosol, S. D. Mittelman, and V. Gilsanz, Reciprocal relation between marrow adiposity and the amount of bone in the axial and appendicular skeleton of young adults, The Journal of Clinical Endocrinology & Metabolism, 2008. 93:2281-2286.

[6] W. Shen, J. Chen, M. Gantz et al, MRI-measured pelvic bone marrow adipose tissue is inversely related to DXA-measured bone mineral in younger and older adults, European Journal of Clinical Nutrition, 2012,66:983-988,

[7] 刘勇,汤光宇,汤榕彪等,^{1}H-MRS 对椎体骨髓研究初步应用[J].实用放射学杂志,2010,26:219-223.
Liu Y, Tang GY, Tang RB, et al. Study of ^{1}H MR spectroscopy of vertebral body marrow. Journal of Practical Radiology, 2010, 26:219-223.

[8] D. Schellinger, C. S. Lin, H. G. Hatipoglu, D. Fertikh, Potential value of vertebral proton MR spectroscopy in determining bone weakness, American Journal of Neuroradiology, 2001, 22: 1620-1627.

[9] Maas M, Akkerman EM, Venema HW, et al Dixon quantitative chemical shift MRI for bone marrow evaluation in the lumbar spine: a reproducibility study in healthy volunteers. J Comput Assist Tomogr. 2001,25:691-7.

[10] Alyas F, Saifuddin A, Connell D. MR imaging evaluation of the bone marrow and marrow infiltrative disorders of the lumbar spine. Magn Reson Imaging Clin N Am. 2007;15:199-219.

[11] Griffith JF, Yeung DK, Antonio GE, Wong SY, Kwok TC, Woo J, Leung PCVertebral marrow fat content and diffusion and perfusion indexes in women with varying bone density: MR evaluation. Radiology. 2006,241:831-838.

[12] T. T. Shih, C. J. Chang, C. Y. Hsu, S. Y. Wei, K. C. Su, and H. W. Chung, Correlation of bone marrow lipid water content with bone mineral density on the lumbar spine, Spine, 2004,29: 2844-2850.

[13] W. Shen, J. Chen, M. Punyanitya, S. Shapses, S. Heshka, and S. B. Heymsfield, MRI-measured bone marrow adipose tissue is inversely related to DXA-measured bone mineral in Caucasian women, Osteoporosis International, 2007, 18: 641-647.

[14] W. Shen, J. Chen, M. Gantz et al, MRI-measured pelvic bone marrow adipose tissue is inversely related to DXA-measured bone mineral in younger and older adults, European Journal of Clinical Nutrition, 2012,66:983-988.

[15] Shen W, Chen J, Punyanitya M, Shapses S, Heshka S, Heymsfield SB MRI-measured bone marrow adipose tissue is inversely related to DXA-measured bone mineral in Caucasian women. Osteoporos Int 2007,18:641-647.

[16] 林帆,李扬彬,谭理连,MR 双回波成像对成人脊柱病变的定量分析,广州医学院学报,2007,35:31-33.
Lin F, Li YB, Tan LL. Quantitative analysis of adult vertebral lesions using dual echo Magnetic Resonance Imaging, Academic

Journal of Guangzhou Medical College, 2007, 35: 31-33.

[17] Gokhan G, Fatma S M, Zeynep Y et al Evaluation of vertebral bone marrow fat content by chemical-shift MRI in osteoporosis Skeletal Radiology. 2011, 40: 577-585.

[18] M. A. Fischer, D. Nanz, A. himakawa, et al. Quantification of muscle fat in patients with low back pain: comparison of multi-echo MR imaging with single-voxel MR spectroscopy, 2013, 1674-1897.

[19] Ojanen X, Borra RJ, Havu M, et al. Comparison of vertebral bone marrow fat assessed by 1HMRSand inphase and out-of-phase MRI among family members. Osteoporos Int, 2013; 2472-9.

(收稿日期: 2014-08-07)

(上接第 686 页)

[2] Denaro V, Longo UG, Denaro L. Vertebroplasty versus conservative treatment for vertebral fractures. Lancet, 2010, 376 (9758): 2071.

[3] Klazen CA, Lohle PN, de Vries J, et al. Vertebroplasty versus conservative treatment in acute osteoporotic vertebral compression fractures (Vertos II): an open-label randomised trial. Lancet, 2010, 376(9746): 1085-1092.

[4] Vargas GE, Mesones RV, Bretcanu O, et al. Biocompatibility and bone mineralization potential of 45S5 Bioglass-derived glass-ceramic scaffolds in chick embryos. Acta Biomater, 2009, 5: 374-380.

[5] Nüchterlein M, Bail HJ. A rare complication of kyphoplasty is PMMA-cement loosening – case report and literature review. Z Orthop Unfall, 2013, 151(5): 463-467.

[6] Verron E, Pissonnier ML, Lesoeur J, et al. Vertebroplasty using bisphosphonate-loaded calcium phosphate cement in a standardized vertebral body bone defect in an osteoporotic sheep model. Acta Biomater, 2014, 10(11): 4887-4895.

[7] Nakano M, Hirano N, Ishihara H, et al. Calcium phosphate cement-based vertebroplasty compared with conservative treatment for osteoporotic compression fractures: a matched case-control study. J Neurosurg Spine, 2006, 4(2): 110-117.

[8] Maestretti G, Sutter P, Monnard E, et al. A prospective study of percutaneous balloon kyphoplasty with calcium phosphate cement in traumatic vertebral fractures: 10-year results. Eur Spine J, 2014, 23(6): 1354-1360.

[9] Blattert TR, Jestaedt L, Weckbach A. Suitability of a calcium phosphate cement in osteoporotic vertebral body fracture augmentation: a controlled, randomized, clinical trial of balloon kyphoplasty comparing calcium phosphate versus polymethylmethacrylate. Spine, 2009, 34(2): 108-114.

[10] Nandi SK, Kundu B, Datta S, et al. The repair of segmental bone defects with porous bioglass: an experimental study in goat. Res Vet Sci, 2008, 2: 162-173.

[11] Bretcanu O, Misra S, Roy I, et al. In vitro biocompatibility of 45S5 Bioglass ((R))-derived glass-ceramic scaffolds coated with poly(3-hydroxybutyrate). J Tissue Eng Regen Med, 2009, 2: 139-148.

[12] Reilly GC, Radin S, Chen AT, et al. Differential alkaline phosphatase responses of rat and human bone marrow derived mesenchymal stem cells to 45S5 bioactive glass. Biomaterials, 2007, 28: 4091-4097.

[13] Lee MH, Ducheyne P, Lynch L, et al. Effect of biomaterial surface properties on fibronectin-alpha (5) beta (1) integrin interaction and cellular attachment. Biomaterials, 2006, 27: 1907-1916.

[14] Xynos ID, Edgar AJ, Buttery LD, et al. Gene-expression profiling of human osteoblasts following treatment with the ionic products of Bioglass 45S5 dissolution. J Biomed Mater Res, 2001, 55(2): 151-157.

[15] Hoppe A, Guldal NS, Boccaccini AR. A review of the biological response to ionic dissolution products from bioactive glasses and glass-ceramics. Biomaterials, 2011, 32(11): 2757-2774.

[16] Reilly GC, Radin S, Chen AT, et al. Differential alkaline phosphatase responses of rat and human bone marrow derived mesenchymal stem cells to 45S5 bioactive glass. Biomaterials, 2007, 28: 4091-4097.

[17] Gerhardt LC, Widdows KL, Erol MM, et al. The pro-angiogenic properties of multi-functional bioactive glass composite scaffolds. Biomaterials, 2011, 32(17): 4096-4108.

[18] Pamula E, Kokoszka J, Cholewa-kowalska K, et la. Degradation, bioactivity, and osteogenic potential of composites made of PLGA and two different sol-gel bioactive glasses. Ann Biomed Eng, 2011, 39: 2114-2129.

(收稿日期: 2015-03-31)